Synthesis and Photocatalytic Activity of Titania Monoliths Prepared with Controlled Macro- and Mesopore Structure

Glenna L. Drisko,*,[†] Andrés Zelcer,[‡,§] Xingdong Wang,[⊥] Rachel A. Caruso,*,[†,⊥] and Galo J. de A. A. Soler-Illia[‡]

[†]Particulate Fluids Processing Centre, School of Chemistry, The University of Melbourne, Parkville VIC 3010, Australia

[‡]Comisión Nacional de Energía Atómica, Gerencia Quimica, Avenida General Paz 1499, San Martín, Provincia de Buenos Aires 1650, Argentina

[§]Escuela de Ciencia y Tecnología (ECyT-UNSAM), San Martín, Provincia de Buenos Aires 1650, Argentina

[⊥]CSIRO Materials Science and Engineering, Private Bag 33, Clayton South VIC 3169, Australia

S *Supporting Information*

ABSTRACT: Herein, we report a one-pot synthesis of crack-free titania monoliths with hierarchical macro-mesoporosity and crystalline anatase walls. Bimodal macroporosity is created through the polymer-induced phase separation of poly(furfuryl alcohol). The cationic polymerization of furfuryl alcohol is performed in situ and subsequently the polymer becomes immiscible with the aqueous phase, which includes titanic acid. Addition of template, Pluronic F127, increases the mesopore volume and diameter of the resulting titania, as the poly(ethylene glycol) block interacts with the titania precursor, leading to assisted assembly of the metal oxide framework. The hydrophobic poly(propylene glycol) micelle core could itself be swollen with monomeric and oligomeric furfuryl alcohol, allowing for mesopores as large as 18 nm. Variations in synthesis parameters affect porosity; for instance furfuryl alcohol content changes the size and texture of the macropores, water content changes the grain size of the titania and Pluronic F127 content changes the size and volume of the mesopore. Morphological manipulation improves the photocatalytic degradation of methylene blue. Light can penetrate several millimeters into the porous monolith, giving these materials possible application in commercial devices.

KEYWORDS: titania, hierarchical pore structures, monoliths, photocatalytic activity, Pluronic F127, furfuryl alcohol

INTRODUCTION

Unclean water, including microbial and chemically polluted water, affects 884 million people, leading to 2.2 million human deaths annually.[1] There is evidence that some herbicides cause human birth defects,[2] as well as reduce the biodiversity of aquatic organisms.[3] It is therefore of utmost importance that a safe, effective and inexpensive means to purify water systems is achieved to protect humans and other creatures from toxic organic pollutants and microbes. Among the strategies put forward, using solar light as a resource is a respected approach to tackle environmental contamination.[1,4]

Titania is a well-known photocatalyst[5,6] and has been used in a good number of applications ranging from self-cleaning surfaces to air and water purification.[7] Titanium dioxide-based photocatalyst materials are nontoxic, abundantly available and inexpensive.[8] The ability to recapture or recycle nanoparticulate materials after a photocatalytic reaction is an issue to be considered. Recently, mesoporous TiO_2 microspheres were developed that were easily separated from the reaction medium, proposing a novel photocatalytic process based on separate adsorption and photocatalytic decomposition steps.[9] This concept can be extended to the production of self-supported monolithic materials, in which the nanostructure of the wall and enhanced surface area are combined with macropores to facilitate fluid diffusion.[10]

Porous inorganic monoliths can be prepared by using preformed templates,[11,12] aerogels,[13,14] polymeric bicontinuous microemulsions,[15,16] spinodal phase decomposition,[17−20] silsesquioxanes bridges,[21,22] or other phase separation induced processes.[23−27] Despite the diversity of synthesis methodologies, obtaining multidimensional pore domains in a simple, inexpensive process from industrial precursors is by no means easy. Such a process that allows simultaneous independent control over two or more pore regimes is a goal pursued by materials scientists.

In this current contribution, we describe a method for the production of titania monoliths presenting high surface area and controlled hierarchical porosity in the micrometer and nanometer range. Colloidal polymeric particles were generated and used as templates in situ. Controlled gelation permitted the preparation of centimeter sized materials,[28] thus avoiding separate steps for template preparation, purification and redispersion. The procedure is commercially viable as it uses

Table 1. Quantity of FA, F127, and H₂O Added to the Synthetic Mixture, Determining x, y, and z[a]

quantity FA			quantity F127			quantity H₂O		
(g)	(mmol)	molar ratio to Ti (x)	(g)	(μmol)	molar ratio to Ti (y)	(g)	(mmol)	molar ratio to Ti (z)
0.00	0.00	0.0	0.00	0.00	0.000	0.00	0.00	0.00
0.32	3.30	1.1	0.04	3.20	0.001	0.03	1.60	0.55
0.64	6.50	2.2	0.10	7.90	0.003	0.06	3.30	1.14
1.28	13.0	4.5	0.21	17.0	0.006			

[a]In each case 6.00 g of TiCl₄/EtOH solution (2.90 mmol Ti) was used.
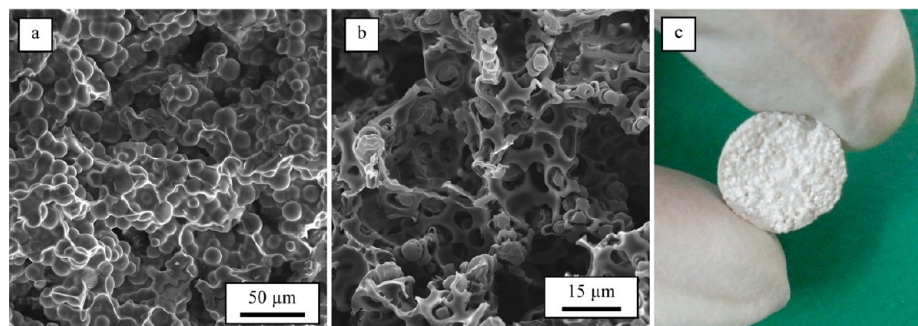

Figure 1. SEM images of 1 Ti:2.2 FA:0.003 F127:0.55 H₂O (a) before and (b) after calcination at 450 °C for 2 h. (c) Titania monolith calcined at 450 °C for 2 h. The radius of the monolith was 1.4 cm and the height was 0.4 cm.

inexpensive materials (titanium tetrachloride, Pluronic F127 and furfuryl alcohol) and is rather insensitive to small variations in the preparation conditions; e.g. temperature and humidity. The sacrificial colloidal template formed macropores of adjustable dimensions; additionally solvent channels were formed creating a second dimension of macropores. Interconnected pores promote diffusion between solutes and the active surface of semiconductors.[29] The mesopore size could be altered by changing the calcination conditions or by adjusting the amount of block copolymer used during the preparation. Increased mesopore size and volume increased the degradation rate of methylene blue, which differs from the findings of previous work.[30,31] Here surface area, crystallite size, crystalline phase, and calcination temperature were decoupled from pore size and volume, showing the importance of well-defined structures for enhanced material performance.

■ EXPERIMENTAL SECTION

Materials. Ethanol (EtOH) and TiCl₄ were purchased from Merck. A 1:40 molar Ti:EtOH stock solution was prepared by dissolving 4.5 g of TiCl₄ in 44 g of ethanol while stirring the vessel in an ice bath (*Warning: heat and HCl vapors evolve!*). Furfuryl alcohol (FA, C₅H₆O₂) and Pluronic F127 (F127) were purchased from Sigma Aldrich. Millipore water ($R > 18$ MΩ cm) was used in all experiments. Reagents were used as received.

Synthesis. Monolithic titania samples were prepared by dissolving F127 in a TiCl₄ solution of ethanol (1:40 molar). Once dissolved, water and FA were added and mixed thoroughly after each addition. The final TiCl₄:EtOH:FA:F127:H₂O molar ratios were 1:40:x:y:z, where x was varied between 0 and 4.5, y between 0 and 0.006, and z between 0 and 1.1. The specific quantities of the reagents added are summarized in Table 1. Samples were stirred in closed vials for 15 min and then left still and open to the environment to allow the solvents to evaporate. After complete gelation, the samples were kept at 60 °C for 5 days then at 130 °C for 3 days. The samples were calcined under a low air flow using the following program: room temperature to 130 °C at 5 °C min⁻¹, 130 to either 350 or 450 °C at a rate of 1 °C min⁻¹, and then the final temperature was held for 2 h.

Photocatalysis Using UV Light. To study the photocatalytic activity of the samples,[32] the finely ground photocatalyst (0.5 g L⁻¹)

was in contact with 160 mL of aqueous methylene blue solution (50 mg L⁻¹) under continuous stirring overnight in the dark to reach adsorption equilibrium. The solution was then placed within a water jacketed reaction chamber at 20 °C and continuously bubbled with air for 30 min to stabilize. A 500 W Hg (Xe) globe (Oriel) with a dichroic mirror (66226, Oriel, 280 < λ < 400 nm) was used to pass light to the solution through a quartz lid. At regular irradiation time intervals (0, 10, 20, 30, 40, 50, and 60 min), aliquots of the solution were withdrawn and centrifuged (15 000 rpm, 10 min, in the dark). The supernatant of these solutions was used to monitor changing methylene blue concentration via UV−vis absorbance spectroscopy (CARY50 Bio UV−visible spectrophotometer).

Characterization. The morphology of the samples was observed by scanning electron microscopy (SEM) performed on a FEI QUANTA 200F microscope operated at voltages between 15 and 20 kV. Samples were mounted on carbon coated SEM stubs and then sputter coated with a thin layer of gold using an Edwards S150B Gold Sputter Coater (30 s sputtering time, 0.5 kV potential). Transmission electron microscopy (TEM) was performed using a Philips CM120 BioTWIN microscope operating at 120 kV. TEM samples were prepared by finely grinding the sample in ethanol using an agate mortar and pestle, sonicating for 20 min and then drop depositing the material on to carbon-coated copper grids.

Nitrogen adsorption−desorption isotherms of whole pieces, several mm in each dimension, were measured. The surface area and pore sizes of the synthesized materials were determined by nitrogen physisorption using a Micromeritics 3000 TriStar instrument at −196 °C. Samples were degassed at 150 °C for at least 2 h prior to analysis using a Micromeritics VacPrep 061. The surface area was calculated using the Brunauer−Emmett−Teller (BET) method. The size distribution of the mesopores was calculated using the Barrett−Joyner−Halenda (BJH) method from the adsorption branch. Mercury intrusion porosimetry was conducted on a Micromeretics AutoPore III with pressure ranging from 2 to 60 000 psi. Samples were degassed at 150 °C before measurement using a Micromeritics VacPrep 061 attached to a heating station. A 14−0411 penetrometer with a bulb size of 3 mL was loaded with the sample. The data was collected and analyzed using Win9420 V1.01.

To determine the crystal structure, the samples were finely ground and X-ray diffraction (XRD) patterns were collected from 10 to 80° 2θ on a Siemens D500 diffractometer equipped with a curved graphite crystal monochromator and a Scintag X1 diffractometer fitted with a

4124

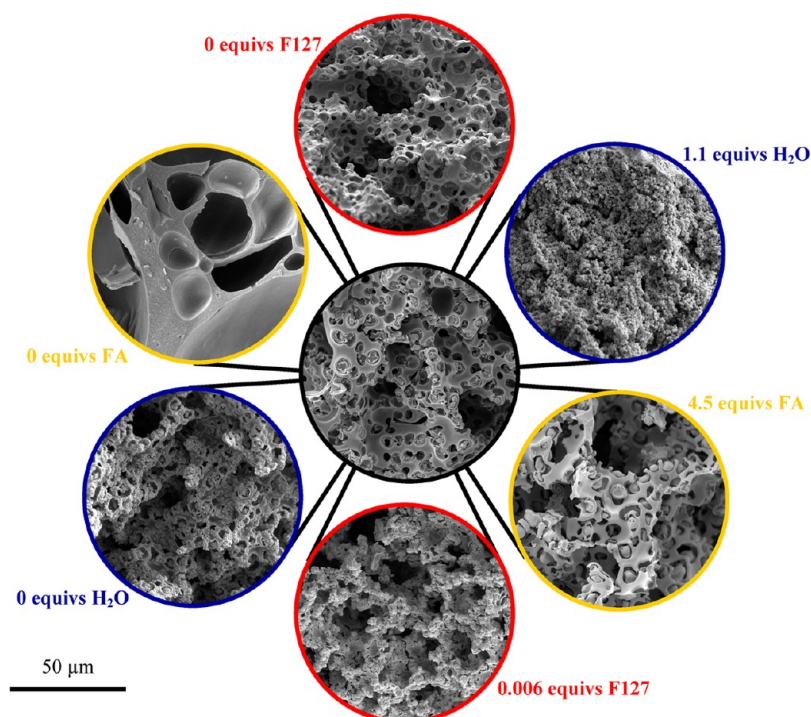dx.doi.org/10.1021/am300880q | ACS Appl. Mater. Interfaces 2012, 4, 4123−4130

Figure 2. SEM images of titania monoliths with varying synthesis conditions. The synthetic molar ratio was 1 Ti:1.1 FA:0.003 F127:0.55 H_2O except where otherwise noted, where "equivs" stands for equivalents to Ti. All samples were calcined at 450 °C for 2 h. The scale is the same for all images.

Peltier detector. Copper K_α radiation at 40 kV and 30 mA was used with a step size of 0.02° 2θ and an integration time of 1 s per step. Crystal size was calculated using the Scherrer equation and the anatase (101) peak at 25.32° 2θ.

RESULTS AND DISCUSSION

The one-pot preparation of titania monoliths is flexible, giving rise to a variety of morphologies by tuning the solution synthesis conditions. Furfuryl alcohol is an α-hydroxymethyl substituted furan that is polymerized and cross-linked through an acid-catalyzed polycondensation, as discussed in detail by Choura et al.[33] Furfuryl alcohol is miscible with the aqueous phase (ethanol, water, the PEG chain of F127 and titanic acid), whereas polyfurfuryl alcohol (PFA) is not and phase separates into colloidal particles. These then act as templates for titania, which gels around the PFA and the block copolymer. Figure 1 shows the morphology of the PFA/titania hybrid and the metal oxide matrix after template removal via calcination. Channels produced from the volume occupied by water/ethanol at the time of titania gelation appear broader after calcination. The formation mechanism is a combination of polymerization-induced phase separation,[34,35] block copolymer templating and inorganic gelification, which has been previously schematically depicted.[28] The principle underlying this synthetic procedure is the decoupling of sol−gel condensation, organic polymer-ization, and self-assembly processes, allowing multiscale texturization.[28,36]

SEM micrographs of the samples before and after calcination show that individual PFA particles are encased in metal oxide (Figure 1). An interconnected void lattice is not observed as is seen in colloidal crystal templating, where particles are in direct contact before precursor infiltration and gelation.[11] The encasement of the PFA is due to the polyethylene glycol (PEG) block of F127 extending from the surface of the polymer colloid. The hydrophobic polypropylene glycol (PPG)

block is more compatible with the PFA spheres. PEG can complex $Ti(OH)_4$ precursors and Ti-oxo building blocks,[37,38] leading to complexation around individual PFA particles and finally, encased cavities or macrovoids. These macrocavities collapse and open during calcination, suggesting either that they are not fully connected to the mesoporous network at the time of gelation, or that the forces during contraction are strong enough to open the structure.

Means to control the structure can be studied and the limits of this method can be found by varying each parameter individually. Changes in the structure and physical properties occurred when the water, F127 and FA content in the initial solution were varied (Figure 2, Table 2). All samples, calcined

Table 2. Physical Properties of Samples Prepared with Varying Solution Compositions As Determined by Nitrogen Sorption; All Samples Were Calcined at 450 °C for 2 h

solution composition	surface area ($m^2\ g^{-1}$)	pore volume ($cm^3\ g^{-1}$)	crystal size $(nm)^a$
1 Ti:0.0 FA:0.003 F127:0.55 H_2O	70 ± 1	0.18 ± 0.01	14.7
1 Ti:1.1 FA:0.003 F127:0.55 H_2O	78 ± 3	0.15 ± 0.01	13.2
1 Ti:4.5 FA:0.003 F127:0.55 H_2O	48 ± 2	0.08 ± 0.01	15.8
1 Ti:1.1 FA:0.000 F127:0.55 H_2O	46 ± 1	0.08 ± 0.01	13.6
1 Ti:1.1 FA:0.006 F127:0.55 H_2O	79 ± 1	0.29 ± 0.01	12.8
1 Ti:1.1 FA:0.003 F127:0.00 H_2O	66 ± 3	0.17 ± 0.02	14.0
1 Ti:1.1 FA:0.003 F127:1.10 H_2O	75 ± 1	0.17 ± 0.02	14.2

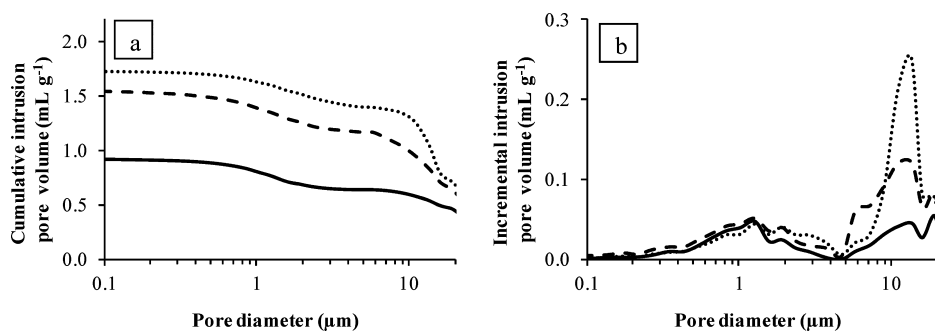^{a}Calculated using the Scherrer equation and the anatase (101) peak at 25.32° 2θ.

Figure 3. Mercury intrusion porosimetry plots (logarithmic scale on *x*-axis) of (a) cumulative intrusion volume vs pore diameter and (b) incremental intrusion vs pore diameter of 1 Ti:*x* FA:0.003 F127:0.55 H$_2$O, where *x* = 1.1 (solid line), 2.2 (dotted line), and 4.5 (dashed line), calcined at 450 °C for 2 h.
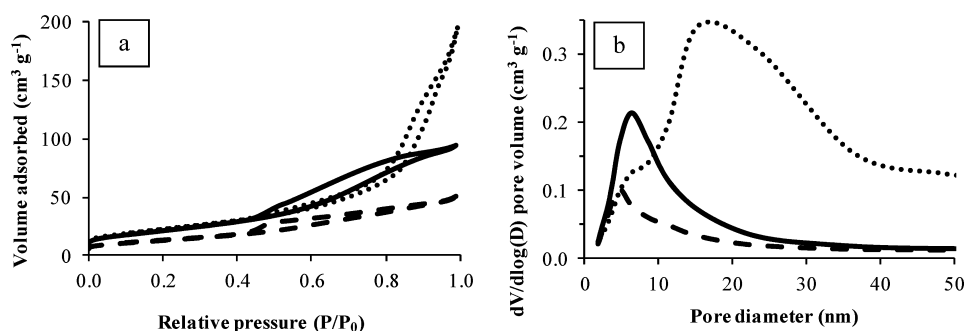

Figure 4. (a) Nitrogen sorption isotherms and (b) pore size distribution curves for 1 Ti:1.1 FA:*y* F127:0.55 H$_2$O where *y* = 0 (dashed line), 0.003 (solid line) and 0.006 (dotted line), calcined at 450 °C for 2 h.

at 450 °C for 2 h, were anatase titania (see Figure S1 in the Supporting Information). Without the use of FA, large solvent channels were still present, but the smaller, spherical macroporous domains were absent. The quantity of FA changed the morphology of the solvent channels as particles of PFA, surrounded by titania, seemed to cluster together during the drying step. At low quantities of block copolymer, discrete particles of PFA formed and were templated. However, as the F127/Ti ratio increased to 0.006, the surface tension was changed and the size of the PFA particles decreased substantially. This effect arose as the surfactant compatibilized the aqueous and polymer phases. The quantity of water changed the grain size of the material. Water quantity is directly related to the condensation degree of the building blocks and thereby changes the interaction with the PEG block.[39] Moreover, the polarity of the solvent increases with increasing water content. At high polarity (H$_2$O/Ti ratio 1.1) the hydrophobic PFA was completely excluded from the titania network and PFA templating was not observed. The truest templating of both the F127 and PFA structure was observed for conditions of 1 Ti:2.2 FA:0.003 F127:0.55 H$_2$O, which will be analyzed in further detail in the following sections.

Effect of FA on Macroporosity. The change in macroporosity was quantitatively measured using mercury intrusion porosimetry (Figure 3). FA/Ti ratios of 1.1, 2.2, and 4.5 in the initial synthesis solution were measured. The cumulative pore volume increased substantially upon doubling this ratio from 1.1 to 2.2. However, increasing the ratio from 2.2 to 4.5 led to a decrease in cumulative pore volume. Samples produced with FA/Ti = 4.5 showed a crust of organic material that disappeared upon calcination. By FA/Ti = 4.5, the synthesis solution was supersaturated in FA; therefore, the polymer was excluded from the network as titania gelation occurred, and

thus maximum macropore volume was obtained for FA/Ti = 2.2.

Effect of F127. Mesopore volume and diameter measured using nitrogen sorption (Figure 4) showed a peak at ~6 nm for all samples, which can be attributed to an interparticle pore (i.e., textural porosity). A second pore population, signaled by a distinct peak, begins to appear upon the addition of F127. This peak shifts toward larger pore diameters as the F127 concentration increases. Normally, F127 templated pores display a pore diameter of ~4−7 nm,[40,41] but it has been noted that monomeric or oligomeric FA can increase the F127 mesopore size by swelling the micelles.[28] When FA was present, changing F127/Ti ratio also changed mesopore diameter (Figure 4b). Under standard F127 templating conditions, that is a system containing water, ethanol, oxide precursor and F127, the mesopore diameter does not deviate with changing F127 concentration,[42] rather it is the phase behavior that changes. It is known that polymeric swelling agents can increase pore size when used in conjunction with nonionic block copolymers.[43] Here, we report for the first time that in the presence of an agent capable of swelling the micellar cores (i.e., FA/oligomeric PFA), the mesopore size can be increased by changes in the F127/inorganic ratio. By doubling the concentration from a F127/Ti ratio of 0.003 to 0.006, the mesopore diameter increased from ~8 nm to ~18 nm. Moreover, the mesopore volume increased steadily with increasing block copolymer concentration (Table 2). Further increases in F127 concentration were not explored because when the F127/Ti ratio was over 0.006, the PFA-templated domains tended to be lost, as seen in Figure 2. In such a complex synthetic route, cross effects exist, and therefore a high F127 quantity increases the PFA solubility in solution, losing the capacity for macropore templating. However, the
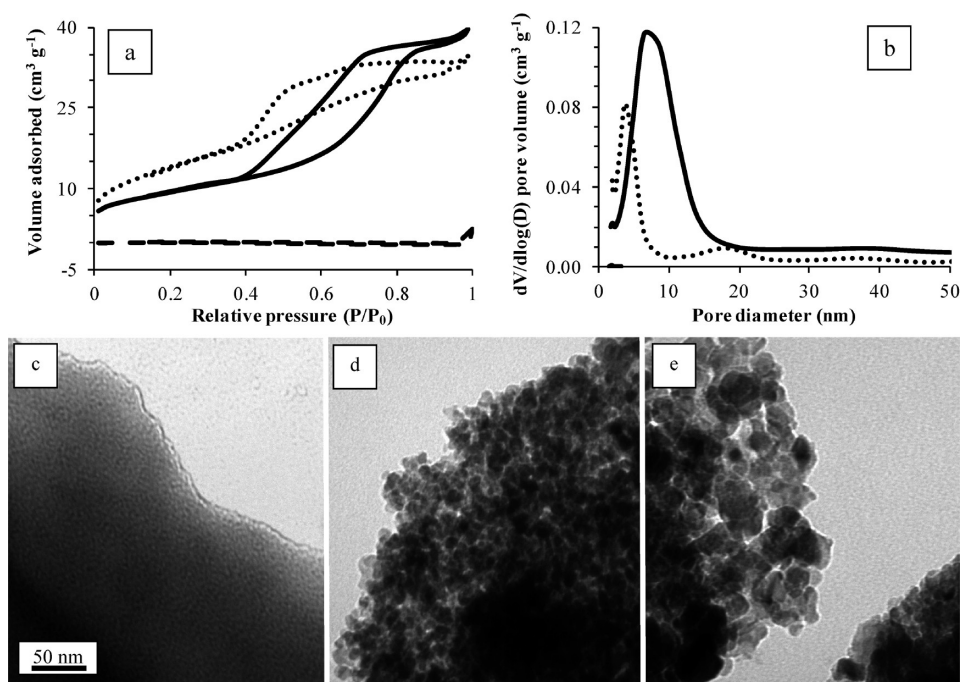
Figure 5. (a) Nitrogen sorption isotherms and (b) BJH pore size distribution (from the adsorption branch) of 1 Ti:1.1 FA:0.001 F127:0.55 H_2O samples prior to calcination (dashed line), after calcination at 350 °C (dotted line), and after calcination at 450 °C (solid line) for 2 h. TEM images of the same material (c) prior to calcination, (d) after calcination at 350 °C, and (e) after calcination at 450 °C for 2 h. The scale is the same for images c, d, and e.

substantial increase in porosity observed for the maximum tested ratio of F127/Ti = 0.006 already can have a significant influence on surface accessibility to solutes.[44]

Effect of Water. Before the addition of FA, the very low pH (generated by partial $TiCl_4$ alcoholysis) and the substoichiometric quantity of water prevent the extensive hydrolysis and condensation of the titanium ions, which under these conditions are mostly complexed by ethoxide and chloride.[45] As the polymerization of FA takes place, water is gradually released into the system and small inorganic clusters begin to grow. The high acidity prevents the extensive condensation of Ti(IV) even in the presence of water, and only small titanium-oxo clusters are formed. These inorganic oligomers act as nanobuilding blocks (NBB) that assemble and condense to produce the final monolithic material. NBB coordinate to the functional groups of the growing colloidal surfaces, forming a shell of a composite inorganic−organic material around the growing macrotemplates. After polymerization of the organic monomer is complete, the titania coating grows in thickness with the incorporation of water from the environment and evaporation of HCl and ethanol, producing a titania/PFA hybrid. Key to the success of this method is the use of $TiCl_4$ as a precursor because the acidity generated from its hydrolysis controls the condensation rate. Initial efforts to produce monoliths using titanium tetraethoxide as a precursor led to the formation of disconnected macropores (data not shown).

Effect of Calcination. The mesopore texturation was investigated by altering the calcination conditions. Nitrogen sorption isotherms and corresponding BJH mesopore size distributions are shown for materials prior to calcination and calcined at 350 and 450 °C (Figure 5a, b). The calcined samples show a strong hysteresis loop from relative pressures of P/P_0 = 0.4−1.0, indicating the presence of both meso- and macropores, whereas noncalcined samples present a small

hysteresis loop in the macropore region, demonstrating negligible micro- and mesoporosity.[46] Presumably before calcination, organic matter occupies the space that becomes mesopores on pyrolysis of the polymers. The sample calcined at 450 °C had less microporosity than that treated at 350 °C, as evidenced from the lower pore volume at $P/P_0 \leq 0.1$. The higher calcination temperature results in higher crystallinity and a higher degree of condensation, as expected. Measurements on finely ground and monolithic (~ 0.3 cm^3) samples have equivalent pore size distributions and surface areas (see Figure S2 in the Supporting Information), demonstrating that the surface and pore volume of the monolith are equally accessible to nitrogen as the powdered sample. The highly accessible surface before grinding is due to the large solvent channels and bimodal macroporosity, which is a clear advantage for exchange or adsorption purposes.

TEM images (Figure 5c−e) supplement the nitrogen sorption data, showing the development of textural porosity (interparticle pores) and larger particle diameters with increasing temperature of calcination. At higher calcination temperatures the necks of the pores are bigger, visually illustrating why the larger pore size distribution is observed in nitrogen sorption analysis. Images of the noncalcined samples look compact, showing very small pin points of lighter contrast. The noncalcined sample contains the organic materials PFA and F127. The organic and inorganic components are distinguishable with TEM as titanium has a higher atomic number to carbon, and therefore affects the electron path to a differing degree. Some wormhole-like mesostructure is present prior to calcination even in samples prepared with the low F127/Ti ratio of 0.001 (see ref 28 for F127/Ti ratio of 0.005). The particles grow during calcination with particle diameters of 10 - 15 nm for the sample calcined at 350 °C and 20−40 nm for samples calcined at 450 °C. The
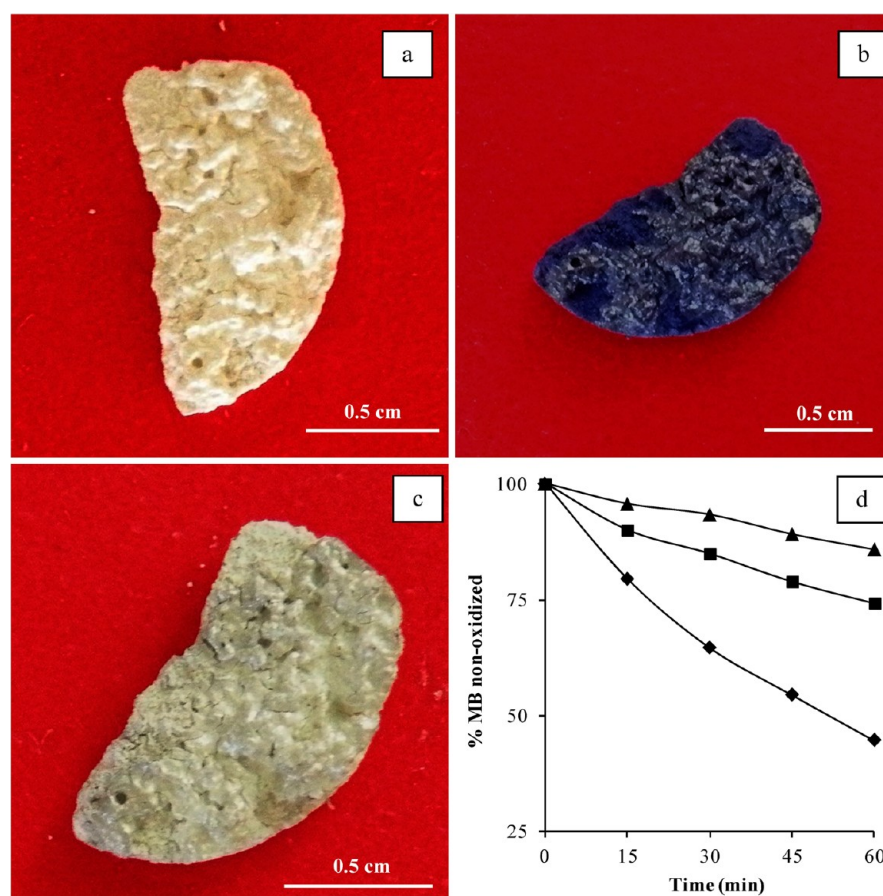
Figure 6. Photographs of the color change (a) before exposure to methylene blue, (b) after adsorption of the blue dye for 1 h, and (c) after 2 h exposure to UV light by a sample prepared with 1 Ti:1.1 FA:0.006 F127:0.55 H_2O. (d) UV-light degradation of methylene blue (MB) by 1 Ti:1.1 FA:y F127:0.55 H_2O, where y = 0 (triangles), 0.003 (squares), and 0.006 (diamonds).

range of the mesopore size distribution of these materials, estimated using the BJH model on nitrogen adsorption data, was: 1.7−2.2 nm for the noncalcined sample, 2−7 nm for the sample calcined at 350 °C and 3−15 nm for the sample calcined at 450 °C. All organic material is removed by 350 °C; the increase in pore size is due to larger pore necks. The pores are formed from interparticle voids rather than block copolymer templating. Despite the loss of templated mesoporosity, F127 has a vital role in directing the morphology of the amorphous material (Figure 4), which seems to have an effect on the crystallization behavior of samples during calcination.

Photocatalytic Activity of the Titania Network. The adsorption and photocatalytic decomposition of methylene blue by titania was demonstrated on a halved monolith. The titania pellet was placed in a concentrated methylene blue solution (50 mg L^{-1}) in the dark for a few minutes, and then removed. The dark blue color of the monolith indicated a large amount of dye was taken into the pores and onto the surface.[47] The material was placed under a UV light for 2 h. The degradation of adsorbed methylene blue, resulting in color loss, within monoliths can be seen with the bare eye (Figure 6c), indicating there is a significant depth of light penetration, as the maximum diffusion of oxidizing radical species is ~10 nm.[48]

The titania materials were tested for photocatalytic activity by measuring the decrease in methylene blue concentration over time (Figure 6d). Samples prepared with different concentrations of F127, H_2O, and FA were studied. The only

parameter that had a significant effect on the rate of methylene blue degradation was the concentration of F127 used during the preparation; the higher the concentration used, the better the material performed as a photocatalyst (Figure 6d). The surface area greatly increased from 46 m^2 g^{-1} for samples prepared without use of F127, to 78 m^2 g^{-1} for materials with an F127/Ti ratio of 0.003 (Table 2). A further increase of block copolymer did not change surface area within the accuracy of measurement (79 m^2 g^{-1} for the case of F127/Ti ratio of 0.006), thus the increase in degradation cannot be attributed merely to surface area. The crystallite sizes for samples with varying F127 content were between 12.8 and 13.6 nm, which are not significantly dissimilar. However, the increase in F127/Ti ratio from 0.003 to 0.006 led to a dramatic increase in pore volume, from 0.15 to 0.29 cm^3 g^{-1}, and mesopore size, from 8 to 18 nm (see Table 2 and Figure 4). It can also be observed that the desorption curve for the sample prepared with higher F127/Ti ratio was shifted to larger P/P_0 values. If we consider that the nitrogen sorption isotherms belong to Type IV, with H2 type hysteresis loops, this increase can be attributed to an increase in the interpore neck sizes.[49]

This observation suggests that for long diffusion pathways, in which transport of the model pollutants and reaction products can be hindered because of tortuosity, the presence of a more developed mesopore system with larger pores and interpore necks should facilitate both transport and surface accessibility. Thus, we can attribute the improved photocatalytic activity observed with increasing F127 concentration to increased

4128

dx.doi.org/10.1021/am300880q | ACS Appl. Mater. Interfaces 2012, 4, 4123−4130

surface contact, both physically and due to the kinetic turnover of reactants and products. Our previously reported hierarchically porous titania monoliths templated from agarose gel reached 49% methylene blue degradation ((initial concentration-final concentration)/initial concentration) within 60 min,[32] whereas the best material here 1 Ti:1.1 FA:0.006 F127:0.55 H_2O, reached 55% over the same time frame. This, in addition to the evidence we report in the current article, proves that the simple presence of hierarchy within a material is not enough and each pore scale should be optimized and tailored for the operating conditions.

CONCLUSIONS

Hierarchically porous TiO_2 monoliths with highly crystalline walls and well-defined macropores and mesopores were prepared by a one-pot colloidal templating method. The method is straightforward, robust, and uses industrial precursors. The mesoporosity can be tuned by altering the F127/Ti ratio or calcination temperature. Macropore volume is affected by the FA/Ti ratio. Addition of large quantities of water (H_2O/Ti = 1.10) interferes with the templating process, but small amounts (H_2O/Ti = 0.55) improve the assembly due to the formation of small titania nanobuilding blocks.

Increasing F127/Ti ratio augments photocatalytic activity, due to increased mesopore size and volume. Light was able to penetrate the top millimeters of the monolith, proving the accessibility of these structures. Macroscopic materials with photocatalytic activity that extends beyond the surface could be used in commonplace water and air purification systems due to the practicality of the macroscopic size and tunable pore structures.

ASSOCIATED CONTENT

Ⓢ Supporting Information

XRD patterns of the reported materials and nitrogen sorption isotherms of a monolith before and after grinding. This material is available free of charge via the Internet at http://pubs.acs.org.

AUTHOR INFORMATION

Corresponding Author
*E-mail: glenna.drisko@upmc.fr (G.L.D.); rcaruso@unimelb.edu.au (R.A.C.).

Notes
The authors declare no competing financial interest.

ACKNOWLEDGMENTS

REFERENCES

(1) Byrne, J. A.; Fernandez-Ibañez, P. A.; Dunlop, P. S. M.; Alrousan, D. M. A.; Hamilton, J. W. J. *Int. J. Photoenergy* **2011**, *798051*, doi: 10.1155/2011/798051.
(2) Stillerman, K. P.; Mattison, D. R.; Giudice, L. C.; Woodruff, T. J. *Reprod. Sci.* **2008**, *15*, 631−650.
(3) Relyea, R. A. *Ecol. Appl.* **2005**, *15*, 618−627.
(4) Malato, S.; Fernández-Ibáñez, P.; Maldonado, M. I.; Blanco, J.; Gernjak, W. *Catal. Today* **2009**, *147*, 1−59.
(5) Fujishima, A.; Honda, K. *Nature* **1972**, *238*, 37−38.
(6) Linsebigler, A. L.; Lu, G. Q.; Yates, J. T. *Chem. Rev.* **1995**, *95*, 735−758.
(7) Fujishima, A.; Zhang, X. T.; Tryk, D. A. *Surf. Sci. Rep.* **2008**, *63*, 515−582.
(8) Carp, O.; Huisman, C. L.; Reller, A. *Prog. Solid State Chem.* **2004**, *32*, 33−177.
(9) Araujo, P. Z.; Luca, V.; Bozzano, P. B.; Bianchi, H. L.; Soler-Illia, G. J. A. A.; Blesa, M. A. *ACS Appl. Mater. Interfaces* **2010**, *2*, 1663−1673.
(10) Wang, X.; Caruso, R. A. *J. Mater. Chem.* **2011**, *21*, 20−28.
(11) Stein, A.; Li, F.; Denny, N. R. *Chem. Mater.* **2008**, *20*, 649−666.
(12) Sotiropoulou, S.; Sierra-Sastre, Y.; Mark, S. S.; Batt, C. A. *Chem. Mater.* **2008**, *20*, 821−834.
(13) Dutoit, D. C. M.; Schneider, M.; Baiker, A. *J. Catal.* **1995**, *153*, 165−176.
(14) Carn, F.; Colin, A.; Achard, M.-F.; Deleuze, H.; Sanchez, C.; Backov, R. *Adv. Mater.* **2005**, *17*, 62−66.
(15) Jones, B. H.; Lodge, T. P. *Chem. Mater.* **2011**, *23*, 4824−4831.
(16) Jones, B. H.; Lodge, T. P. *Polym. J.* **2012**, *44*, 131−146.
(17) Hasegawa, G.; Morisato, K.; Kanamori, K.; Nakanishi, K. *J. Sep. Sci.* **2011**, *34*, 3004−3010.
(18) Konishi, J.; Fujita, K.; Nakanishi, K.; Hirao, K. *Chem. Mater.* **2006**, *18*, 864−866.
(19) Hasegawa, G.; Kanamori, K.; Nakanishi, K.; Hanada, T. *J. Am. Ceram. Soc.* **2010**, *93*, 3110−3115.
(20) Nakanishi, K.; Tanaka, N. *Acc. Chem. Res.* **2007**, *40*, 863−873.
(21) Kanamori, K.; Nakanishi, K. *Chem. Soc. Rev.* **2011**, *40*, 754−770.
(22) Brandhuber, D.; Peterlik, H.; Hüsing, N. *Small* **2006**, *2*, 503−506.
(23) Vantomme, A.; Léonard, A.; Yuan, Z.-Y.; Su, B.-L. *Colloids Surf., A* **2007**, *300*, 70−78.
(24) Hardy Dessources, A.; Hartmann, S.; Baba, M.; Hüsing, N.; Nedelec, J. M. *J. Mater. Chem.* **2012**, *22*, 2713−2720.
(25) Gutiérrez, M. C.; Ferrer, M. L.; del Monte, F. *Chem. Mater.* **2008**, *20*, 634−648.
(26) Deville, S. *Adv. Eng. Mater.* **2008**, *10*, 155−169.
(27) Drisko, G. L.; Chee Kimling, M.; Scales, N.; Ide, A.; Sizgek, E.; Caruso, R. A.; Luca, V. *Langmuir* **2010**, *26*, 17581−17588.
(28) Drisko, G. L.; Zelcer, A.; Luca, V.; Caruso, R. A.; Soler-Illia, G. J. A. A. *Chem. Mater.* **2010**, *22*, 4379−4385.
(29) Aprile, C.; Corma, A.; Garcia, H. *Phys. Chem. Chem. Phys.* **2008**, *10*, 769−783.
(30) Kim, D. S.; Han, S. J.; Kwak, S.-Y. *J. Colloid Interface Sci.* **2007**, *316*, 85−91.
(31) Yu, J. C.; Wang, X.; Fu, X. *Chem. Mater.* **2004**, *16*, 1523−1530.
(32) Wang, X.; Mitchell, D. R. G.; Prince, K.; Atanacio, A. J.; Caruso, R. A. *Chem. Mater.* **2008**, *20*, 3917−3926.
(33) Choura, M.; Belgacem, N. M.; Gandini, A. *Macromolecules* **1996**, *29*, 3839−3850.
(34) Müller, H.; Rehak, P.; Jäger, C.; Hartmann, J.; Meyer, N.; Spange, S. *Adv. Mater.* **2000**, *12*, 1671−1675.

(35) Grund, S.; Seifert, A.; Baumann, G.; Baumann, W.; Marx, G.; Kehr, M.; Spange, S. *Microporous Mesoporous Mater.* **2006**, *95*, 206−212.

(36) Drisko, G. L.; Zelcer, A.; Caruso, R. A.; Soler-Illia, G. J. A. A. *Microporous Mesoporous Mater.* **2012**, *148*, 137−144.

(37) Soler-Illia, G. J. A. A.; Sanchez, C. *New J. Chem.* **2000**, *24*, 493.

(38) Hechavarría, L.; Mendoza, N.; Altuzar, P.; Hu, H. *J. Solid State Electrochem.* **2010**, *14*, 323−330.

(39) Kajihara, K.; Yao, T. *J. Sol−Gel Sci. Technol.* **1998**, *12*, 193−201.

(40) Yamada, T.; Zhou, H.; Asai, K.; Honma, I. *Mater. Lett.* **2002**, *56*, 93−96.

(41) Grosso, D.; Soler-Illia, G. J. A. A.; Babonneau, F.; Sanchez, C.; Albouy, P.-A.; Brunet-Bruneau, A.; Balkenende, A. R. *Adv. Mater.* **2001**, *13*, 1085−1090.

(42) Bagshaw, S. A.; Prouzet, E.; Pinnavaia, T. J. *Science* **1995**, *269*, 1242−1244.

(43) Malfatti, L.; Bellino, M. G.; Innocenzi, P.; Soler-Illia, G. J. A. A. *Chem. Mater.* **2009**, *21*, 2763−2769.

(44) Drisko, G. L.; Imperia, P.; de los Reyes, M.; Luca, V.; Caruso, R. A. *Langmuir* **2010**, *26*, 14203−14209.

(45) Crepaldi, E. L.; Soler-Illia, G. J. A. A.; Grosso, D.; Cagnol, F.; Ribot, F.; Sanchez, C. *J. Am. Chem. Soc.* **2003**, *125*, 9770−9786.

(46) Sing, K. S. W.; Everett, D. H.; Haul, R. A. W.; Moscou, L.; Pierotti, R. A.; Rouquerol, J.; Siemieniewska, T. *Pure Appl. Chem.* **1985**, *57*, 603−619.

(47) Fan, X.; Fei, H.; Demaree, D. H.; Brennan, D. P.; St. John, J. M.; Oliver, S. R. L. *Langmuir* **2009**, *25*, 5835−5839.

(48) Carretero-Genevrier, A.; Boissiere, C.; Nicole, L.; Grosso, D. *J. Am. Chem. Soc.* **2012**, *134*, 10761−10764.

(49) Lowell, S.; Shields, J. E.; Thomas, M. A.; Thommes, M. *Characterization of Porous Solids and Powders: Surface Area, Pore Size and Density*; Springer: Amsterdam,2010.